Topological network-assisted quantum operations in two-dimensions

MSc COSSE Literature Review

by

Genya G. Crossman
Student number 5607728

25 April, 2022

Thesis committee
Prof. Eliška Greplová
Prof. Kees Vuik

Contents

1 Introduction

1.1 Overview

Scientific computing and applied mathematics enable the exploration of and, sometimes even, the simplification of complex systems through various optimized modeling and simulation methods. These fields create and utilize computational resources to do so. Many problems, however, are still unsolvable or very difficult to solve with current well-established methods – be it algorithms or computers. Quantum computers were theorized and are now being realized to extend computational abilities. Though commercially available and widely researched, quantum computers today are still more proof-of-concept than "universally" applicable tools. A major part of the problem is these systems are riddled with noise, hence the phrase noisy intermediate scale quantum (NISQ) devices is commonly used to refer to current day devices. There are many approaches to mitigating the effects of noise in quantum systems from both hardware and software perspectives. This work focuses on optimizing the device hardware by combing aspects of two already well-explored systems – superconducting quantum integrated circuits and topological insulators.

The former are relatively easy to fabricate and have become one of the main focuses of today's industry, including competitive involvement from IBM and Google [1, 2]. The heart of superconducting quantum circuits is found in two circuit elements: the quantum bit (qubit) and the resonator. The qubit manages quantum information processing. The resonator is a simple inductor and capacitor (LC) in parallel and is a well understood classical circuit element. Resonators play a key role in this proposed research. In contrast, topological quantum systems are incredibly difficult to fabricate, having only recently been demonstrated for the first time by Microsoft [3]. In theory, however, topological insulators promise a strong shield against noise across the device [4]. By leveraging the simplicity and ease of simulating classical LC resonators and combining this with the noise-protection introduced in topological systems, this work will develop a model supporting how such a hybrid hardware could process and protect quantum information [5].

The end goal is to understand how a two-dimensional array of resonators could behave as a qubit when demonstrating the topological property known as edge modes (see Figure 1) [5]. This will be done by considering how to optimize these edge modes such that there is enough control of the circuit to run single qubit gates. Understanding how to control these modes, though, requires a familiarity with the theory behind quantum integrated circuits, circuit quantum electrodynamics (CQED), as well as the importance of energy band gaps and symmetries in topological systems. After an introduction to these topics, an overview of experimental evidence of edge modes on pendula (the mechanical equivalent to LC resonators) is presented as motivation for how to demonstrate edge modes in classical resonator systems [6]. Finally, this project's goal is addressed in more detail. Prior to any of the particularities of this proposed work, though, it is useful to become familiar with some standard notation,

vocabulary, and visualization methods of quantum computing.

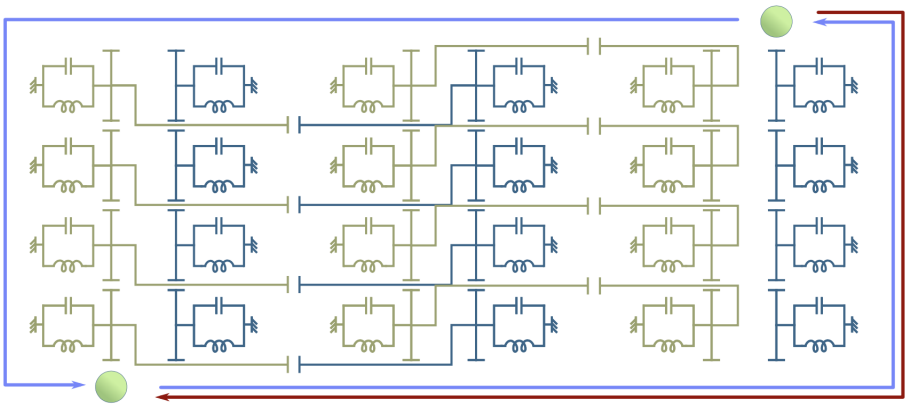

Figure 1: A sketch of the proposed hardware. A two-dimensional array of resonators, which is designed in such a way as to demonstrate topological edge modes, is attached to two control qubits. The two edge modes of the array act as ground and excited states, causing the array to behave like a qubit itself [5]. Image is from Greplová (2021) [5].

1.2 Bra-Ket/Dirac Notation

Quantum mechanics is, in its mathematical essence, an elegant discussion around linear algebra. Quantum states are represented by vectors and operators by matrices. Often times these states and operators are commonly found throughout many different quantum systems, so rather then re-write the lengthy linear algebraic representation, the bra-ket notation is used. This is also known as Dirac notation. In this a vector is written as a ket, shown as

$$\vec{0} = |0\rangle = \begin{bmatrix} 1 \\ 0 \end{bmatrix} \tag{1}$$

This state is known as the ground state of a qubit, whereas

$$|1\rangle = \begin{bmatrix} 0 \\ 1 \end{bmatrix} \tag{2}$$

is the excited state [7]. Note that a qubit only has two energy states of interest – $|0\rangle$ and $|1\rangle$ – in the same way that its classical counterpart, the bit, only considers 0 and 1; if more states are accessible then it is no longer a qubit, e.g. a qutrit actively considers gates on $|0\rangle$, $|1\rangle$, and $|2\rangle$ [7]. When discussing the superconducting qubit called a transmon, as in section 2.3, however, the $|2\rangle$ state is included in some calculations as the energetic boundary whose condition

must be considered to understand the two lower energetic states of interest. The conjugate transpose, or Hermitian conjugate, of a ket is known as a bra, or

$$\vec{0}^H = \vec{0}^* = \vec{0}^\dagger = \langle 0| = \begin{bmatrix} 1 & 0 \end{bmatrix} \tag{3}$$

A bra and ket put immediately next to each other represent an inner product [7]. It is easy to see, then, that $\langle x|x\rangle = 1$ for any state $|x\rangle$ and that $\langle x|y\rangle = 0$ for any orthogonal states $|x\rangle$ and $|y\rangle$. Though it may seem superfluous to recreate a notation for already well-established linear algebraic methods, this notation greatly simplifies equations when considering larger systems beyond a single qubit. For example, given a two qubit system of qubits a and b, the state of the whole system could be written as the tensor product of the two respective states [7].

$$|a\rangle \otimes |b\rangle = |a\rangle\,|b\rangle = |ab\rangle \tag{4}$$

Operators, of which quantum gates are a subset, are often denoted with a hat and represent matrices. One example of a quantum gate acting on a single qubit is the X gate

$$\hat{X} = \sigma_x = \begin{bmatrix} 0 & 1 \\ 1 & 0 \end{bmatrix} \tag{5}$$

which will flip the qubit it acts on from $|0\rangle$ to $|1\rangle$ and vise versa. This is also known as the Pauli matrix σ_x and is known in classical computing as the NOT gate [7]. As quantum gates have common labels (e.g. X, Y, Z, H, CNOT, etc.), the hat notation highlighting their responsibility as operators is dropped. The X gate is also defined as a rotation of π about the x-axis of the Bloch sphere, which is useful tool for visualising the evolution of a single qubit's state.

1.3 Bloch Sphere and Single Qubit Gates

If one drew a connection between the two possible values of a classical bit, it would be a line as there are only two possibilities: 0 or 1. Though a qubit can be 0 or 1 (written in Dirac notation that is $|0\rangle$ or $|1\rangle$), it also can be what is called a superposition of the two states, or rather some combination of the two

$$|\psi\rangle = \alpha\,|0\rangle + \beta\,|1\rangle \tag{6}$$

where $\alpha, \beta \in \mathbb{C}$. The tricky thing with quantum information, however, is that it cannot be directly observed. If one were to measure $|\psi\rangle$ in Equation 6, one would get the result $|0\rangle$ with probability of $|\alpha|^2$ or $|1\rangle$ with probability of $|\beta|^2$ [7]. The probabilities of measurement must sum to 1, $|\alpha|^2 + |\beta|^2 = 1$, implying that $|\psi\rangle$ is normalized, much like a unit vector [7]. When expressing the state in terms of spherical coordinates, any global phase is ignored as it has no physical significance [7].

$$|\psi\rangle = \cos\left(\frac{\theta}{2}\right)|0\rangle + e^{i\varphi}\sin\left(\frac{\theta}{2}\right)|1\rangle \tag{7}$$

θ is the angle from the z-axis and φ is the angle from the x-axis. With this, it is easy to see that qubit state $|\psi\rangle$ can be anywhere on the Bloch sphere's surface

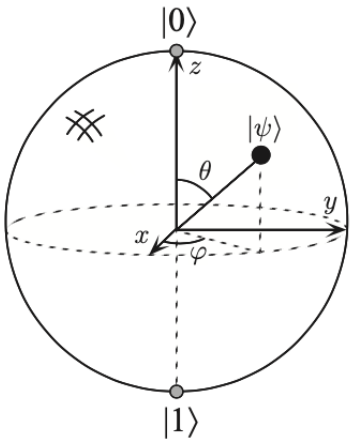

Figure 2: The Bloch sphere helps visualize how the state of a single qubit evolves. The north pole is the ground state and the south pole is the excited state. Where a classical bit could only exist on these poles, the qubit's state, $|\psi\rangle$, can be anywhere on the the surface of the sphere. Image is from Nielson and Chuang (2010) [7].

(see Figure 2). This is a very easy way to see how single qubit gates affect a state. Let's revisit the example of the X gate in Equation 5 to see this clearly.

When an X gate is applied on a quantum state, the state flips about the x-axis of the Bloch sphere. For example, if $|\psi\rangle = |0\rangle$ to start and an X gate is applied, then $|\psi\rangle = |1\rangle$.

$$X|0\rangle = \begin{bmatrix} 0 & 1 \\ 1 & 0 \end{bmatrix} \begin{bmatrix} 1 \\ 0 \end{bmatrix} = \begin{bmatrix} 0 \\ 1 \end{bmatrix} = |1\rangle \tag{8}$$

Similarly, $X|1\rangle = |0\rangle$ [7]. The Z gate is similar and is defined by it's Pauli matrix.

$$Z = \sigma_z = \begin{bmatrix} 1 & 0 \\ 0 & -1 \end{bmatrix} \tag{9}$$

In this case, $Z|0\rangle = 0$ and $Z|1\rangle = -1$ [7]. There is also a Y gate, which behaves in a similar fashion to the X and Z. What is even more interesting, is the Hadamard gate, H, which is known for generating a superposition state.

$$H = \frac{1}{\sqrt{2}} \begin{bmatrix} 1 & 1 \\ 1 & -1 \end{bmatrix} \tag{10}$$

where

$$\begin{aligned} H|0\rangle &= \frac{|0\rangle + |1\rangle}{\sqrt{2}} \\ H|1\rangle &= \frac{|0\rangle - |1\rangle}{\sqrt{2}} \end{aligned} \tag{11}$$

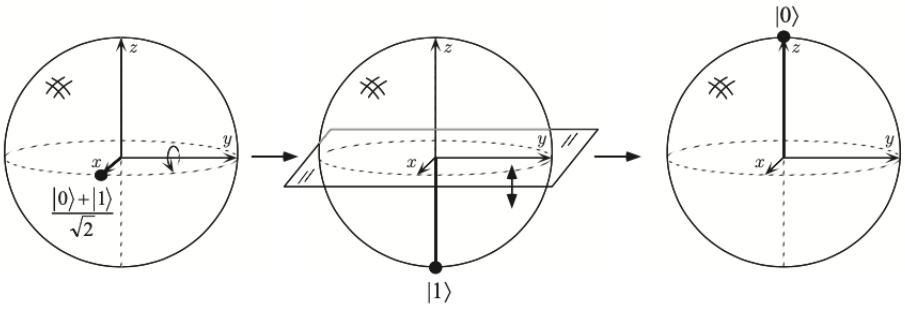

Figure 3: A Hadamard gate acting on initial state $\frac{|0\rangle+|1\rangle}{\sqrt{2}}$ results in final state $|0\rangle$. The evolution of the state is marked by the black dot in each frame. Image is from Nielson and Chuang (2010) [7].

These superposition states are on either end of the x-axis of the Bloch sphere. If a Hadamard gate is run on a qubit that is already in a superposition state directly along the x-axis, for example $\frac{|0\rangle+|1\rangle}{\sqrt{2}}$, then the gate causes the state to return to $|0\rangle$, as is demonstrated in Figure 3. In this way, applying two Hadamard gates to initial state $|0\rangle$ results in an identical final state, i.e. $H^2 = \mathbb{I}$ [7]. This is in contrast to the other gates, where $XX^\dagger = ZZ^\dagger = \mathbb{I}$. This touches upon the single rule for quantum gates: they must be unitary [7].

While mapping quantum gates on the Bloch sphere is useful, it does not explain how to actually run gates on quantum hardware. The goal of this project is to determine a model for how to represent single qubit gates – namely the X, Z, and H gates – on the new, proposed hardware. As the proposed hardware is rooted in superconducting qubits, it is useful to understand the foundational theory behind that field, namely, CQED.

2 Circuit QED

2.1 Overview

Superconducting quantum circuits have become one of the central quantum hardwares of today largely for the ease in fabrication and scalability. These devices are made based on well-established lithography processes. Nonetheless, it is still difficult to properly model and fabricate these systems, specifically related to a particular circuit element crucial to creating a qubit: the Josephson junction (JJ). JJs determine the frequency of a qubit and, thus, if and how it will interact with its neighbors. This project's proposed array of resonators would bypass this problem. Resonators are easier to model and are more robust against fabrication errors compared to JJs. If the proposed concept of using a two-dimensional array of resonators as a qubit (rather than the commonly used transmon, which contains JJs) works well, then it would be easier to simulate and build more reliable and larger quantum systems. The motivation for how a block of resonators could behave as a qubit is rooted in work done by Süsstrunk and Huber (2015) and requires an understanding of topological systems [6]. This will be addressed in the next chapter. Prior to that, though, it is important to understand how resonators themselves work, as well as how a special type of superconducting qubit called a transmon works and how these two elements and their interaction can be described by the Jaynes-Cummings Hamiltonian.

2.2 Lumped Element Resonators

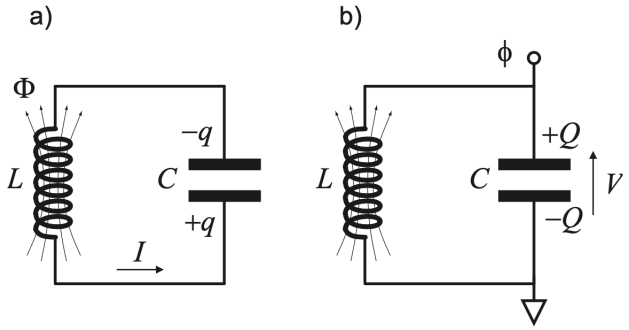

Figure 4: The LC resonator is comprised of an inductor, L, and capacitor, C, in parallel. On the left-hand side, the system is expressed in terms of flux about the inductor, charge across the capacitor, and current, I; whereas on the right-hand side, the system is explained by a flux, ϕ, at the node north of the capacitor and a voltage, V, across the capacitor. Both diagrams portray the same system, but expressed with different degrees of freedom: charge and flux on the left and right respectively. Image is from Girvin (2014) [8].

Resonators in circuit QED are often called cavities, a term that was borrowed from cavity QED. These circuit elements behave as harmonic oscillators and are traditionally used to read out qubit states without probing and, thus, disturbing the quantum information directly. In this project, however, resonators are considered for a different purpose: to generate a new kind of qubit more robust to environmental noise. Resonators can be considered protectors of quantum information in integrated circuits. Though they typically have been used to protect quantum information from destruction, we explore how they may also further protect quantum information from noise.

When it comes to microwave engineering and superconducting quantum circuits, there are two common types of resonators used: lumped element resonators and coplanar waveguides. The former will be the focus of this project, though exploration into the latter may prove interesting for future work.

A lumped element resonator is comprised of an inductor, L, and a capacitor, C, in parallel (see Figure 4), forming a simple electrical LC harmonic oscillator. The name "lumped element" refers to the fact that the physical size is much smaller than the associated wavelength and that the voltage and current are relatively steady across the element [9]. The Lagrangian of such a resonator is

$$\mathcal{L} = \frac{LI^2}{2} - \frac{q^2}{2C} \tag{12}$$

where q is the charge of the capacitor and I is the inductor's current. Recalling from charge conservation that $I = \dot{q}$, which means the Lagrangian may be rewritten as

$$\mathcal{L} = \frac{L}{2}\dot{q}^2 - \frac{1}{2C}q^2 \tag{13}$$

Now this looks remarkably similar to the classical problem of a mass on a string; here, instead of distance the degree of freedom is charge, rather than mass there is inductance, and the inverse capacitance replaces the spring constant [8]. This similarity is not only incredibly helpful for further analysis of resonators, but will come into play again in section 3.3. Following the Euler-Lagrange equation of motion $\frac{\partial \mathcal{L}}{\partial q} - \frac{d}{dt}\frac{\partial \mathcal{L}}{\partial \dot{q}} = 0$ equation 13 becomes

$$\ddot{q} = -\frac{1}{LC}q = -\omega_r^2 q \tag{14}$$

where $\omega_r = \frac{1}{\sqrt{LC}}$ is the natural frequency of the resonator [8]. $\frac{\partial \mathcal{L}}{\dot{q}}$ defines the conjugate or generalized momentum [10], which, as seen in equation 13, is $L\dot{q}$ or LI, also known as the inductor's flux, Φ [8]. The resonator's Hamiltonian is then expressed as

$$H = \Phi\dot{q} - \mathcal{L} = \frac{\Phi^2}{2L} + \frac{1}{2C}q^2 \tag{15}$$

If, however, the flux of the node next to the capacitor, ϕ, see Figure 4, is used as the degree of freedom instead of charge and the negative charge, $Q = -q$, becomes the conjugate momentum, then the Hamiltonian may be expressed as

$$H = Q\dot{\phi} - \mathcal{L} = \frac{1}{2C}Q^2 + \frac{\phi^2}{2L} \tag{16}$$

In either case, by following the canonical commutation relation, the degree of freedom and the conjugate momentum may be expressed as operators that are Fourier transforms of each other

$$[\hat{q}, \hat{\Phi}] = i\hbar = [\hat{\phi}, \hat{Q}] \tag{17}$$

Now equation 16 can be expressed in terms of raising and lowering operators [8].

$$\begin{aligned} \hat{a} &= i\frac{1}{\sqrt{2C\hbar\omega_r}}\hat{Q} + \frac{1}{2L\hbar\omega_r}\hat{\phi} \\ \hat{a}^\dagger &= -i\frac{1}{\sqrt{2C\hbar\omega_r}}\hat{Q} + \frac{1}{2L\hbar\omega_r}\hat{\phi} \\ [\hat{a}, \hat{a}^\dagger] &= 1 \end{aligned} \tag{18}$$

Now the Hamiltonian of the resonator can be written as [8]

$$H = \frac{\hbar\omega_r}{2}(a^\dagger a + aa^\dagger) = \hbar\omega_r(a^\dagger a + \frac{1}{2}) \tag{19}$$

Expressing the resonator Hamiltonian in terms of raising and lowering operators will come up again when the Jaynes-Cummings Hamiltonian is discussed, which explains the interactions between qubits and resonators.

LC resonators are often referred to as quantum harmonic oscillators as they can be expressed by an evenly spaced (harmonic) potential energy well. This means that the energy levels of a resonator are evenly spaced by $\hbar\omega_r$. Qubits, however, should only have two energy levels, the ground and first excited state, as was discussed in the introduction; therefore, transmons – a commonly used type of superconducting qubit – are anharmonic quantum oscillators, meaning they have unevenly space energy levels. This allows access to the first two energy levels in isolation from the rest (see Figure 5). Next, a deeper understanding of the transmon is presented.

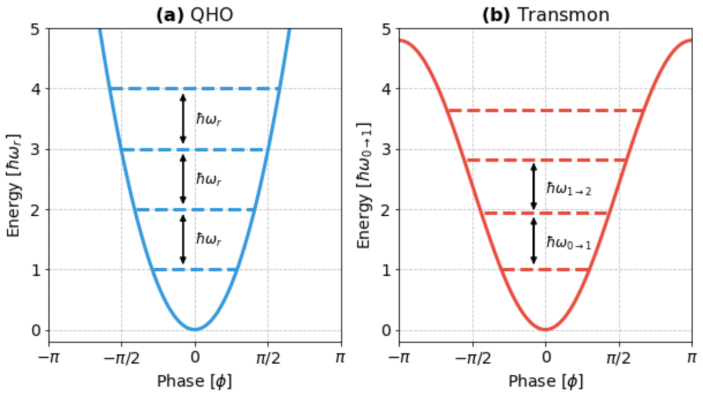

Figure 5: The energy potentials for a quantum harmonic oscillator (resonator) and transmon. The former shows energy levels evenly spaced by $\hbar\omega_r$, where ω_r is the frequency of the resonator. The transmon energy levels are unevenly spaced. They depend on the frequency associated with transitioning between each respective energy level, e.g. the gap between the first two levels is proportional to $\omega_{0\to1}$, the frequency of the transmon transitioning from the ground to the first excited state. Other spacings between energy levels are not proportional to this same frequency, though. Image is from Hoffer (2021) [11].

2.3 Transmon and Jaynes-Cummings Hamiltonian

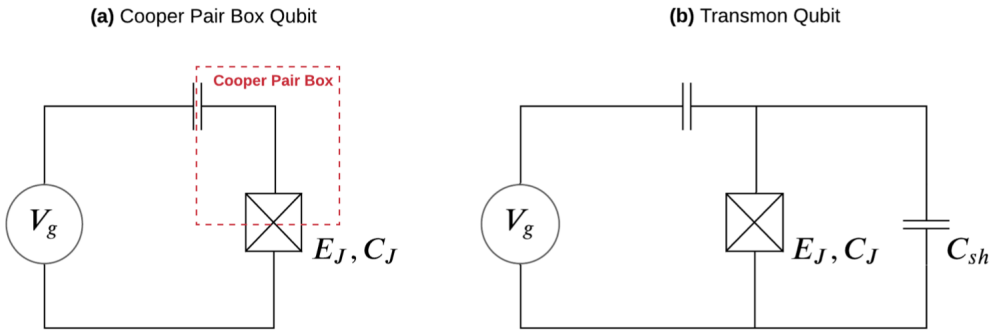

Figure 6: The Cooper pair box circuit (left) is the same as the LC resonator, but with the inductor of the resonator replaced by a Josephson junction, which is marked by the box with an x in it. The transmon circuit (right) is similar to the Cooper pair box, but includes a shunt capacitor, C_{sh}, to minimize charge noise. E_J and C_J refer to the Josepshon energy and capacitance respectively [11, 12]. Image is from Hoffer (2021) [11].

Superconducting qubits grew out of a simple arrangement referred to as the Cooper pair box, which looks like the LC resonator already discussed, but with a JJ replacing the inductor (see Figure 6). "The Josephson junction is the only known dissipationless non-linear circuit element" [12]. As previously discussed, if one considers the simple LC resonator, as introduced in section 2.2, with a Josephson junction replacing the inductor, then the harmonic oscillations become non-linear, meaning that its associated energy levels are no longer evenly spaced. Thus, if the Cooper pair box is engineered with specific capacitance and inductance, then the energy levels can be designed in such a way where the first two states are within frequency range of experimental interest (gigahertz) and the higher energy bands are out of range [12]. With the first two non-linear energy levels – the ground state, $|0\rangle$, and first excited state, $|1\rangle$ – accessible, this circuit element now behaves as a physical qubit when cooled down to roughly 10mK and manipulated with microwave pulses.[1]

The transmon is a widely used updated version of the Cooper pair box in that it is less sensitive to charge noise compared to its predecessor [12]. It is characterized by the ratio of its Josephson energy, E_J, to its charging energy, E_C. The former relates to when a pair of spin-1/2 particles tunnel across the JJ. This tunneling generates "charge difference" between the two capacitors of

[1] Please note that the word "physical" is consciously included as often times when quantum computers are discussed in terms of use cases, the size or number of qubits is described in terms of logical qubits. A single logical qubit is made of several physical qubits along with some error correcting code to mitigate natural, unavoidable errors that arise in the system. As this project is considering hardware and not quantum algorithms, when qubits are mentioned the implication is that they are physical qubits, not logical ones.

the JJ, thus determining the qubit state [12]. Charging energy, on the other hand, relates to the total capacitance of the transmon $E_C = \frac{e^2}{C_{sh}+C_J}$ [11, 12]. Transmons have a ratio of Josephson energy to charging energy such that $\frac{E_J}{E_C} > 4$ [12]. Increasing E_J/E_C decreases tunneling and the charge noise across the junction [12]. For this reason, some researchers use $\frac{E_J}{E_C} = 50$ [11]. The bare qubit frequency – i.e. the frequency of a single qubit in isolation, not coupled to any other qubits or resonators – is also dependent on the Josephson and charge energies, $\omega_q \approx \sqrt{8E_J E_C}$ [11].

Josephson and charge energy also help describe a transmon's rate of interaction with a resonator, often called the coupling, g [12].

$$g_{i,j} = \sqrt{2}g(\frac{E_J}{8E_C})^{1/4} \langle i| (b - b^\dagger) |j\rangle \tag{20}$$

b and $b^\dagger$ are the raising and lowering operators of the qubit, while $|i\rangle$ and $|j\rangle$ refer to the two qubit states of interest. If these two states are nearest neighbors, then this expression simplifies to the following [12].

$$g_{j,j+1} = g(\sqrt{2(j+1)}(\frac{E_J}{8E_C})^{1/4}) \tag{21}$$

Though it is nice to express the coupling between a qubit and resonator, what is measured is actually another parameter called the dispersive shift, χ, which is expressed in terms of the coupling, as well as the difference between qubit and resonator frequencies, $\Delta = \omega_{ij} - \omega_r$. ω_{ij} is the frequency of a qubit shifting between states $|i\rangle$ and $|j\rangle$. Δ is often called the detuning. As qubits cannot be measured directly without destroying their quantumness, they are attached to resonators. A resonator is then measured and if its frequency has shifted slightly, it is indication that it is attached to a qubit. This shift marks not only the presence of a qubit, but also which state the qubit is in and how strongly coupled the resonator and qubit are. This shift is the dispersive shift. If the resonator's frequency decreases by χ then the qubit is in the ground state whereas if it increases by χ, then the qubit is in the excited state.

$$\chi_{ij} \equiv \frac{g_{ij}^2}{\Delta_{ij}} \tag{22}$$

Using equation 20, then this becomes

$$\chi_{ij} = 2\sqrt{\frac{E_J}{8E_C}} \frac{g^2 |\langle i| (b - b^\dagger) |j\rangle|^2}{\Delta_{ij}} \tag{23}$$

To further simplify things, an effective dispersive shift can be defined as follows [12].

$$\chi_{eff} = \chi_{01} + \frac{\chi_{12} + \chi_{02}}{2} \propto \frac{g^2}{\Delta} \tag{24}$$

The effective dispersive shift is useful for properly expressing the effective Hamiltonian of the single qubit-single resonator system.

$$H_{eff} = \frac{\hbar(\omega_{01} + \chi_{01})}{2} + \hbar((\omega_r - \chi_{01} - \chi_{02}) + \chi_{eff}\sigma_z)a^\dagger a \tag{25}$$

This expresses the state of the qubit in the first term and the resonator in the second term with a and $a^\dagger$ as the lowering and raising operators associated with the photon or resonator, as was noted in section 2.2. The $\chi_{eff}\sigma_z$ term represents the interaction between the two elements. This Hamiltonian is commonly referred to as the Jaynes-Cummings Hamiltonian and is visulaized using a "ladder" as seen in Figure 7 [12].

Superconducting qubit-resonator systems are excited and controlled using microwave pulses. That is how qubit gates are run and, consequently, how qubit states are changed. In this project the new proposed qubit is actually a bunch of resonators and we are considering to excite this array using transmons. In this way microwave pulses may excite the transmon(s) attached to the resonator array and consequently excite the edge modes of the resonator array. Modeling this proposed process requires an understanding of edge modes and, thus, properties often associated with topological insulators.

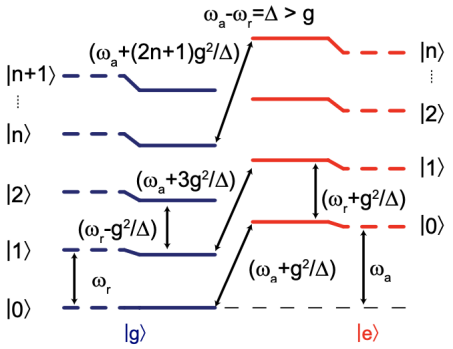

Figure 7: Interactions described by the Jaynes-Cummings Hamiltonian of a single qubit and resonator pair can be represented in a ladder schematic. The blue lines on the left represent when a qubit with bare frequency ω_a is in the ground state, $|g\rangle$, and the red lines are when it is in the excited state, $|e\rangle$. The dashed lines represent the uncoupled Hamiltonian's eigenstates, whereas the solid lines are the energies when considering coupling. $|n\rangle$ is the photon number. Note that a true qubit would only consider the first two states, $|0\rangle$ and $|1\rangle$, but higher order levels are included for completeness. This image considers the situation known as the dispersive limit, where $\omega_a - \omega_r = \Delta > g$; g is the coupling between qubit and resonator. In this scenario, the "effective" resonator and qubit frequencies shift. The bare qubit and resonator frequencies are shown by both ω_a and ω_r marked by the lower most vertical arrows between $|0\rangle$ and $|1\rangle$ depicting the frequencies in terms of the uncoupled states. The shifted frequencies associated with the coupled system are noted in terms of coupling and detuning, $\frac{g^2}{\Delta}$. This also refers to the dispersive shift, χ. These shifted frequencies are marked by the arrows relating the solid lines. When the qubit is in the ground state, the resonator's frequency decreases slightly (as is seen in the shift between the dashed and solid blue lines at $|1\rangle$). In contrast, when the qubit is in the excited state, the resonator's frequency increases (as is seen in the shift between the dashed and solid red lines at $|1\rangle$). Image is from Schuster (2007) [12].

3 Topological quantum systems

Although this project focuses on the behavior of quantum circuits, it is motivated by properties commonly found in topological systems, particularly the appearance and robustness of edge modes along a lattice. While traditionally these edge modes appear in quantum systems, they have recently also been demonstrated on an array of classical mechanical oscillators that displayed two modes in the clockwise and counter-clockwise directions [6]. As LC resonators are the electrical equivalent to mechanical oscillators, we believe achieving such edge states on a two-dimensional array of resonators is also possible. Topologically non-trivial systems can host edge modes. For a system to be topological, there must be an energy band gap between what is considered the physical bulk of the system versus its edges and symmetry projection must be present. If both of these conditions are upheld, the system will be exceptionally robust to perturbations, or rather any noise occurring in the environment.

To understand the fundamentals between the edges and bulk and the preservation of symmetry, we first consider a one-dimensional lattice of particles. This scenario is explained by the Su-Schrieffer-Heeger (SSH) model. Though the proposed work is not in one-dimension and, thus, cannot directly utilize the SSH model, the SSH model is a simpler, perhaps even more intuitive presentation of the importance of energy band gap and chiral symmetry. A further analysis of topological systems continues with a focus on a more directly relevant model: the quantum spin Hall effect (QSHE) [13]. For this, a quick introduction to time-reversal symmetry and Kramers pairs is provided. Finally, a review of Süsstrunk and Hubers' (2015) work demonstrating chiral edge modes on mechanical oscillators is presented [6]. This serves as a guidance for how to set up the Hamiltonian of our proposed LC resonator system.

3.1 SSH Model

The SSH model describes the topological behavior of a one-dimensional chain of particles or atoms. A common physical example for which the SSH model applies is polyacetylene [15]. Polyacetylene is a chain of carbon atoms, each with one hydrogen atom hanging off. When the chain is broken up into sites – each with one unique pair of carbon atoms – then two types of general bonds can be identified: inter- and intra-site bonds, whose strengths are denoted w and v respectively [14, 16]. These are shown as a single (w) and double (v) line connecting the carbon atoms in Figure 8. Thus, a single site or unit cell is comprised of one atom on the bottom connected to one atom on top by a double line (v). All "bottom" ("top") particles comprise what is considered a sublattice. Each sublattice's particles do not interact with one another. A particle can only interact with its nearest neighbor, which is of opposite sublattice type (i.e. top only interacts with its nearest neighbor bottom particles and vise versa). This sublattice symmetry is the SSH model's chiral symmetry [14, 16]. It is useful to note that this scenario considers non-interacting electrons, thus each electron can be considered a single particle [16]. The Hamiltonian for such a system is

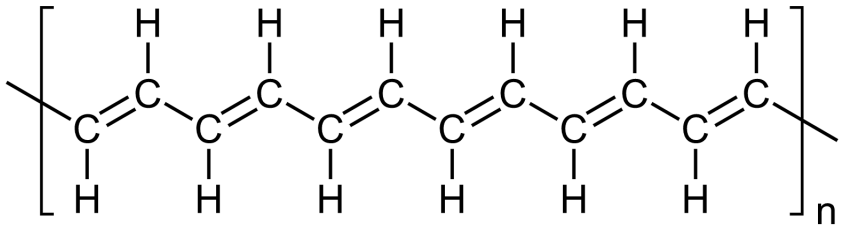

Figure 8: A chain of carbon atoms known as polyacetylene is a common physical example of the SSH model. Atoms are categorized into sub-lattices. This is demonstrated by the staggering of the lattice showing half the particles on "top" and half on "bottom." One unit cell is comprised of one particle from each sublattice, i.e. one "top" and one "bottom." The bond of two atoms within a cell is denoted by a double line and is referred to as v. The intercell bonds are shown as a single line and called w. v and w are referred to as hopping amplitudes [14].

given as

$$\begin{aligned} H = v \sum_{m=1}^{N} |m, B\rangle \langle m, A| + |m, A\rangle \langle m, B| \\ + w \sum_{m=1}^{N-1} |m+1, B\rangle \langle m, A| + |m, A\rangle \langle m+1, B| \end{aligned} \tag{26}$$

where N is the number of sites in the chain and A and B (what was previously referred to as top and bottom) denote which sublattice, as seen in Figure 8 [16].

The Pauli exclusion principle requires that no two fermions, or spin-half particles, which includes electrons, exist in the same state at the same time in the same system [17]. Given no potential energy and zero temperature, this means all eigenstates of the SSH Hamiltonian are limited to single occupancy as each cite has one particle of each spin; this is also known as half-filling [16]. Expressing the Hamiltonian in terms of internal and external degrees of freedom will become useful as the system is described in terms of bulk and edges. The internal degree of freedom indexes the unit cells and the external degree of freedom identifies the sublattices [16]. These are m and α respectively, such that $|m, \alpha\rangle = |m\rangle \otimes |\alpha\rangle \in \mathcal{H}_{internal} \otimes \mathcal{H}_{external}$ [16]. Now the SSH Hamiltonian can be written as

$$\begin{aligned} H = v \sum_{m=1}^{N} |m\rangle \langle m| \otimes \hat{\sigma}_x \\ + w \sum_{m=1}^{N-1} |m+1\rangle \langle m| \otimes \frac{\hat{\sigma}_x + i\hat{\sigma}_y}{2} + |m\rangle \langle m+1| \otimes \frac{i\hat{\sigma}_x - \hat{\sigma}_y}{2} \end{aligned} \tag{27}$$

where $\hat{\sigma}_x$ and $\hat{\sigma}_y$ are the Pauli matrices, with $\hat{\sigma}_x$ defined in Equation 5 and

$$\hat{\sigma}_y = \begin{bmatrix} 0 & -i \\ i & 0 \end{bmatrix} \tag{28}$$

In this expression, the hopping amplitudes look like operators on their respective bonds [16].

The Hamiltonian for the bulk should be irrespective of the edges, as the idea that we can distinguish clearly between these two modes is central to topological insulators. The bulk is thus given periodic boundary conditions, letting us effectively treat it as a ring [16]. The bulk Hamiltonian now is

$$\begin{aligned} H_{bulk} = &\sum_{m=1}^{N} v(|m, B\rangle \langle m, A| + |m, A\rangle \langle m, B|) \\ &+ w(|m \mod N+1, A\rangle \langle m, B| + |m, B\rangle \langle m \mod N+1, A|) \end{aligned} \tag{29}$$

where

$$\begin{aligned} H_{bulk} |\Psi_n(k)\rangle = E_n |\Psi_n(k)\rangle, \\ n \in 1, ..., 2N \end{aligned} \tag{30}$$

with wavenumber or, as is more commonly referred to in condensed matter theory, crystal momentum k [14, 16]. As the bulk is translationally invariant, Bloch's theorem allows expressing the state in terms of a plane wave in the first Brillouin zone, $k \in \delta_k, ..., \delta_k N$ where $\delta_k = \frac{2\pi}{N}$,

$$|k\rangle = \frac{1}{\sqrt{N}} \sum_{m=1}^{N} e^{imk} |m\rangle \tag{31}$$

with Bloch eigenstates $|\Psi_n(k)\rangle$

$$|\Psi_n(k)\rangle = |k\rangle \otimes |u_n(k)\rangle \tag{32}$$

$$|u_n(k)\rangle = a_n(k) |A\rangle + b_n(k) |B\rangle \in \mathcal{H}_{int} \tag{33}$$

$|u_n(k)\rangle$ are the eigenstates of the bulk momentum-space Hamiltonian

$$H(k) |u_n(k)\rangle = E_n(k) |u_n(k)\rangle \tag{34}$$

where

$$\begin{aligned} H(k) &= \langle k| H_{bulk} |k\rangle \\ &= \sum_{\alpha,\beta \in A,B} \langle k, \alpha| H_{bulk} |k, \beta\rangle \cdot |\alpha\rangle \langle \beta| \end{aligned} \tag{35}$$

[16].

The function $u_{n,k}(x)$ (where $\Psi_{n,k}(x) = e^{ikx}u_{n,k}(x)$) demonstrates periodicity in real space, but not in the Brillouin zone; however, the Fourier transform from real space to Brillouin zone is on the external degree of freedom only, thus periodicity in the Brillouin zone is maintained [16].

$$\begin{aligned} H(k+2\pi) &= H(k) \\ |u_n(k+2\pi)\rangle &= |u_n(k)\rangle \end{aligned} \tag{36}$$

The bulk momentum-space Hamiltonian has a zero diagonal. This reflects that there is no interaction among particles within a given sublattice. Particles in an SSH chain only interact with their nearest neighbors [16]. This localized interaction denotes a chiral symmetry in the system. The Hamiltonian can then be written as

$$H(k) = \begin{pmatrix} 0 & v + we^{-ik} \\ v + we^{ik} & 0 \end{pmatrix} \tag{37}$$

Given Equation 34, $H(k)^2 = E(k)^2\hat{\mathbb{I}}_2$,

$$E(k) = \pm|v + we^{ik}| = \pm\sqrt{v^2 + w^2 + 2vwcos(k)} \tag{38}$$

This allows us to see beauty of the SSH model, which arises when the hopping amplitudes v and w are staggered [16]. To fully appreciate when staggered v and w give rise to a topologically invariant system (as opposed to a trivial one), though, the Hamiltonian can be rewritten in terms of something called the d-vector, $\mathbf{d}$(k).

Given $|u_n(k)\rangle \in \mathcal{H}_{internal}$ provides information on the internal structure, the bulk momentum-space Hamiltonian for a system with two states per cite (i.e. two particles per unit cell) can be expressed as

$$\begin{aligned} H(k) &= d_0(k)\hat{\sigma}_0 + d_x(k)\hat{\sigma}_x + d_y(k)\hat{\sigma}_y + d_z(k)\hat{\sigma}_z \\ &= d_0(k)\hat{\sigma}_0 + \mathbf{d}(k)\hat{\sigma} \end{aligned} \tag{39}$$

where

$$\begin{aligned} d_0(k) &= 0 \\ d_x(k) &= v + wcosk \\ d_y(k) &= wsink \\ d_z(k) &= 0 \end{aligned} \tag{40}$$

Thus, the direction of $\mathbf{d}$(k) determines the internal structure of eigenstates and the magnitude of the vector determines the energy. The radius of the circle is of size w and the center sits at v. $\mathbf{d}$(k) must be a closed loop and encircle the origin for the lattice to maintain chiral symmetry and be considered topological [16]. This becomes clear in Figure 9, in which the top row shows energy plotted against wavenumber for varying values of v and w and the bottom row plots the associated $\mathbf{d}$(k) to the image above it. The image to the far right (e) reflects a system in which there is no intra-cell hopping, i.e. the two particles within a unit cell are fully disconnected. In this case it is clear how there would be a

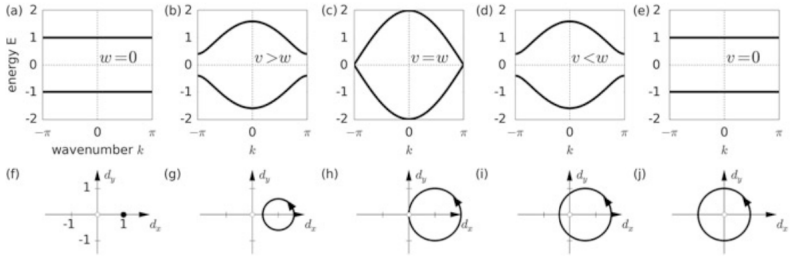

Figure 9: (a) to (e) show the energy as a function of wavenumber for varying relations between inter- and intra-cell hopping amplitudes, w and v: (a) $v = 1, w = 0$, (b) $v = 1, w = 0.6$, (c) $v = w = 1$, (d) $v = 0.6, w = 1$, (e) $v = 0, w = 1$ [16]. The smallest gap between the energy bands is equal to twice the absolute value of the difference between the hopping amplitudes. Note that (c) shows a conductor as the energy bands connect allowing electrical flow without tunneling. In the insulator case, as the gap increases the number of occupied energy states decreases. (f) to (j) show the circular $\mathbf{d}$(k) path for the bulk momentum-space Hamiltonian as k crosses through the Brillouin zone from 0 to 2π for each respective situation shown above in (a) to (e) [16]. Image is from Asbóth, Oroszlány, Pályi (2016) [16].

separation in what is considered the bulk compared to the edges as there is a physical break in the connections. The next image to the left (d) demonstrates a system in which the intra-cell hopping has been slightly turned on, but is still weaker than inter-cell hopping. The particles that were physically separated in (e) on the edges are now connected again; however, the energy band gap is still present and $\mathbf{d}$(k) still encircles the origin. As both chiral symmetry and the energy band gap have been maintained, this still reflects a topological system. The central image (c), however, shows a system in which $v = w$ and, thus, there is closure to the energy band gap. This gap closure demonstrates the topological phase transition between $v < w$ and $v > w$ or rather between the system behaving topologically or trivially. The following systems (a) and (b) restore the band gap, but $\mathbf{d}$(k) no longer contains the origin and, therefore, are considered trivial rather than topological; they no longer display separation in bulk and edge modes [16]. By mapping the energies for various combinations of hopping amplitudes and $\mathbf{d}$(k) of the bulk momentum-space Hamiltonian, we begin to see the significance of bulk versus edge modes.

Figure 10 further emphasizes how when the intra-cell hopping amplitude, v, is turned on and increased, the system still remains topologically invariant until it equals w [16]. This is visible in Figure 10(a), in which there is a line around $E = 0$, which is separate from the rest of the energy spectrum. This line reflects the energy of the edge mode. It starts at 0 when $v = 0$ and increases exponentially as v increases. Recall that when $v = 0$ the edges of the lattice are physically separated from the rest of the system, hence zero energy. The delayed

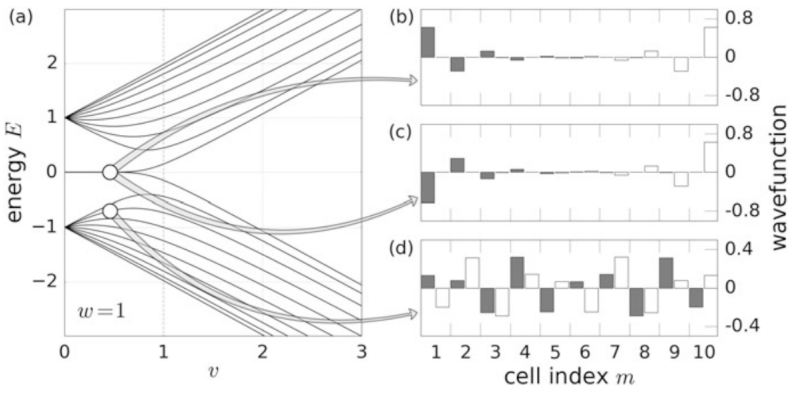

Figure 10: (a) The energy mapped as a function of intra-cell hopping, v, of a ten-cell lattice described by the SSH model with inter-cell hopping $w = 1$. When $v = 0$, the cells along the chain are broken apart, thus creating physically separated edges. As v increases, however, the energy of the edge – denoted by the seemingly horizontal line at $E = 0$ – exponentially increases. Until $v = 1$, the edge cells – though physically connected again – still maintain their own distinguishable energy separate from the bulk of the lattice. After $v = 1$, the distinct edge modes disappear and the system is no longer topological. (b) - (c) These plots highlight how a wavefunction associated with the edge mode in (a) are indeed isolated to the edge cells. (d) When a wavefunction is considered along the bulk of the system, it is spread amongst all cells and not isolated in the same way it is for edges as shown in (b) and (c) [16]. Image is from Asbóth, Oroszlány, Pályi (2016) [16].

union of the edge and bulk modes maintains a gap between the two energies even as v increases (but is still less than w). This allows the system to remain topologically nontrivial. Figure 10(b) and (c) highlight how a wavefunction associated with the zero energy edge modes of the topological system indeed are isolated to the edges. Whereas Figure 10(d) demonstrates how a wavefunction associated with the bulk states is spread across the entire bulk and not isolated to any particular cells in the chain. Once $v = w$, however, and as it continues to increase, the system loses its topological classification and becomes trivial; the edges are indistinguishable energetically from the bulk [16].

After examining this one-dimensional example of the SSH model, it is clear how edge modes can exist in topological systems. It is also clear how maintaining an energy band gap and symmetry is crucial to maintaining topological invariance [16]. Where the SSH model represents these features in terms of hopping amplitudes that have simple-to-understand physical meaning (e.g. the bond strength between two carbon atoms in polyacetylene), other symmetries in higher dimensional systems may not be as obvious at first. One of them, time-reversal symmetry, is certainly not as intuitive as bond strengths, but is

critical for demonstrating the QSHE, which describes how spin-up and spin-down particles can exist in the same system at the same time.

3.2 Time-Reversal Symmetry and Quantum Spin Hall Effect

Symmetry operators, which are unitary, do not disturb the inner product of two states

$$\langle U\psi|U\phi\rangle = \langle\psi|\, U^\dagger U\,|\phi\rangle = \langle\psi|\phi\rangle \tag{41}$$

and, thus,

$$U^\dagger HU = H \tag{42}$$

where H is a Hamiltonian with symmetry U [18]. Anti-unitary symmetry operators, Ω, however, do not preserve inner products and instead produce the complex conjugate [18].

$$\langle\Omega\psi|\Omega\phi\rangle = \langle\phi|\psi\rangle = \langle\psi|\phi\rangle^* \tag{43}$$

Similarly, where symmetry operators are linear $U(\alpha\,|\phi\rangle + \beta\,|\psi\rangle) = \alpha U\,|\phi\rangle + \beta U\,|\psi\rangle$, anti-unitary operators are anti-linear

$$\Omega\alpha\,|\phi\rangle = \Omega\alpha\Omega^{-1}\Omega\,|\phi\rangle = \alpha^*\Omega\,|\phi\rangle = \alpha^*\,|\Omega\phi\rangle \tag{44}$$

where $\alpha \in \mathbb{C}$ [18]. Rather, an anti-unitary operator transforms a complex number into its complex conjugate, which agrees with the same behavior seen in relation to an inner product. Given this, we can say that $\Omega = \mathcal{K}$, where $\mathcal{K}$ is the complex conjugation operator with $\mathcal{K}^2 = \mathbb{I}$ and $\mathcal{K} = \mathcal{K}^{-1}$ [18]. To see how this affects quantum mechanical systems, the simplest thing to do is to consider $\mathcal{K}$ on one-dimensional Schrödinger's equation, $i\hbar\frac{\partial\psi(x,t)}{\partial t} = H\psi(x,t)$

$$Ki\hbar\frac{\partial\psi(x,t)}{\partial t}K = KHK\cdot K\psi(x,t)K \tag{45}$$

$$-i\hbar\frac{\partial\psi^*(x,t)}{\partial t} = H^*\psi^*(x,t) \tag{46}$$

$$i\hbar\frac{\partial\psi^*(x,t)}{\partial - t} = H^*\psi^*(x,t) \tag{47}$$

With $H = H^*$, then $\psi^*(x,t)$ is the solution to the time-reversed one-dimensional Schrödinger's equation [18]. In a system with spin, the Hamiltonian to describe spin orbit coupling is dependent on the Pauli matrices; however, σ_y is not $\mathcal{K}$ invariant [18]. Therefore, to maintain time-invariance for spin systems, another anti-unitary operator, $\mathcal{T}$, is defined [6, 18].

$$\mathcal{T} = i\sigma_y\mathcal{K} \tag{48}$$

When considering how $\mathcal{T}$ works with eigenstates, $\mathcal{T}\,|\psi\rangle = \lambda\,|\psi\rangle$, it becomes evident that it cannot have any [18]. This is seen by adding an extra time-reversal operator, $\mathcal{T}^2\,|\psi\rangle = \mathcal{T}\lambda\,|\psi\rangle$. By definition, the left-hand side should equal $-\,|\psi\rangle$. The right-hand side, however, does not [18].

$$\mathcal{T}^2 |\psi\rangle = \mathcal{T}\lambda |\psi\rangle = \lambda^* \mathcal{T} |\psi\rangle = |\lambda|^2 |\psi\rangle \neq -|\psi\rangle \tag{49}$$

In this way there are two degenerate eigenstates. $|\psi\rangle$ and $|\phi\rangle$ are referred to as a Kramers pair [18].

$$\begin{aligned} \mathcal{T} |\phi\rangle &= -|\psi\rangle \\ \mathcal{T} |\psi\rangle &= |\phi\rangle \end{aligned} \tag{50}$$

These states are orthogonal as

$$\langle \psi | \mathcal{T}\psi \rangle = \langle \mathcal{T}^2 \psi | \mathcal{T}\psi \rangle = -\langle \psi | \mathcal{T}\psi \rangle \tag{51}$$

Additionally, the time-reversal symmetry operator does not have a Hermitian conjugate [18].

$$\langle \psi | \mathcal{T}\phi \rangle \neq \langle \mathcal{T}^\dagger \psi | \phi \rangle \tag{52}$$

This equation would require that the left and right hand sides demonstrate anti-linear and linear relationships, respectively [18].

Applying time-reversal symmetry to a Hamiltonian describing a system with spin demonstrates the existence of a Kramers pair; one eigenstate may be spin up with the other is spin down and while they exist at the same energy, they do not interact. This phenomenon is known as the quantum spin Hall effect [13]. QSHE demonstrates topological systems through time-reversal symmetry. Projecting this concept onto a system of LC resonators, there are two chiral edge modes – clockwise and counter-clockwise – that exist at the same frequency but do not cancel each other out. This application of QSHE in classical oscillators was first demonstrated on a lattice of mechanical pendula by Süsstrunk and Huber (2015) [6]. To understand what the Hamiltonian looks like for a two-dimensional array of LC resonators mimicking the QSHE, it is useful to understand the Hamiltonian for such a mechanical system.

3.3 Quantum Spin Hall Effect in the Classical Realm

The motivation behind finding topological edge modes in LC resonators came from results showing such behavior in a two-dimensional array of pendula coupled by springs [6]. Neither of these systems are ruled by the laws of quantum mechanics, yet given that the electrical oscillators behave in a similar manner to the mechanical ones (see section 2.2), it is believed that such methods can be extended to electrical oscillators. The overview of how such mechanical systems are compared to quantum-associated topological insulators is as follows: QSHE reflects a separation between edge and bulk modes in a system with two degrees of freedom reflecting two spin modes. Classical oscillators naturally only describe systems with one degree of freedom. To remedy this, consider the Hamiltonian describing the classical oscillator system, H_ϕ; when the complex conjugate of the original Hamiltonian, H_ϕ^*, is also included, then requirements for comparing to QSHE are met as there are now two degrees of freedom contained in the whole system's Hamiltonian, H [6, 16, 19]. This is illustrated in

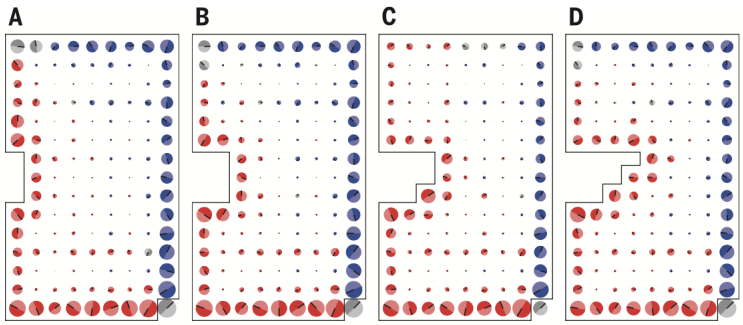

Figure 11: Four deformations of a two-dimensional lattice of pendula are shown. Each deformation of the physical edge is considered a perturbation to the system. The system, however, is undisturbed by such environmental changes as it is topologically protected. The red and blue coloring around the edges denote the two circular edge modes observable after exciting the site furthest to the bottom right. Image is from Süsstrunk and Huber (2015) [6].

equation 53. H_ϕ is taken from Hofstadter's model (see equation 54), which is used in condensed matter theory to describe flux under a very strong magnetic field. Though there is no exceptional magnetic field in the case of mechanical or LC oscillators, there is still a flux acquired from the phase in both systems that can be described the same way as in Hofstadter's model [6, 20]. As the system is mimicking the QSHE on spin-1/2 particles, the associated flux is $\phi = \frac{2\pi}{3}$ [6].

$$\mathcal{H} = \begin{pmatrix} H_\phi & 0 \\ 0 & H_\phi^* \end{pmatrix} \tag{53}$$

$$H_{\alpha,\phi} = f_0 \sum_{r,s,\alpha} |r,s,\alpha\rangle \langle r,s\pm 1,\alpha| + |r,s,\alpha\rangle \langle r\pm 1,s,\alpha| \, e^{\pm i\alpha\phi_s} \tag{54}$$

where α represents what is commonly refered to as the spin of the electron, but here differentiates between H_ϕ and H_ϕ^*. (r,s) designate the location of the cell of interest in the lattice (as is noted in figure 12), f_0 is the hopping amplitude, and $\phi_s = \phi s$ [6]. In this convoluted way, condensed matter theory is used to describe a classical system that exhibits behavior previously expected only of quantum systems.

Now H describes the whole system with two degrees of freedom and it should be possible to see how edge modes arise. The problem, however, is that H is complex, but mechanical oscillators are described by Newton's equation of motion, $\ddot{x_i} = \mathcal{D}_{ij}x_j$, with x the coordinate of the pendula. This expresses a real, not complex system. The Hamiltonian expressing the couplings, $\mathcal{D}$, within the mechanical oscillator array must be real, symmetric, and positive semi-definite. By applying a unitary transformation, U, on H, the classical system is finally described fully as both real and with two degrees of freedom [6]. Equations 55 and 56 demonstrate how this transformation maps the quantum, complex

description of the system (i.e. in terms of Hamiltonian H with $\psi^+_{r,s}$ and $\psi^-_{r,s}$ as the wavefunctions at lattice site (r, s) with spin + or $-$) to the real domain of $\mathcal{D}$ (with $x_{r,s}$ and $y_{r,s}$ representing each pendulum at lattice site (r, s)) [6].

$$U = \frac{1}{\sqrt{2}} \begin{pmatrix} 1 & -i \\ 1 & i \end{pmatrix} \tag{55}$$

$$\begin{pmatrix} x_{r,s} \\ y_{r,s} \end{pmatrix} = \frac{1}{\sqrt{2}} \begin{pmatrix} 1 & 1 \\ i & -i \end{pmatrix} \begin{pmatrix} \psi^+_{r,s} \\ \psi^-_{r,s} \end{pmatrix} \tag{56}$$

where now

$$U^\dagger \mathcal{H} U = \begin{pmatrix} Re\mathcal{H}_\phi & Im\mathcal{H}_\phi \\ -Im\mathcal{H}_\phi & Re\mathcal{H}_\phi \end{pmatrix} \equiv \mathcal{D} \tag{57}$$

The diagonal elements of the coupling matrix, $\mathcal{D}$, represent coupling between two pendula, either xx or yy, or in terms of the language discussed in the SSH model, two atoms on the same sublattice type in neighboring unit cells [6]. Please remember that as we are no longer ruled by the SSH model, this type

Figure 12: Two mechanical oscillators attached by a series of pairs of springs. The two oscillators create one site or cell in the same way that two carbons create a unit cell in polyacetylene chain. Image is from Süsstrunk and Huber (2015) [6].

of coupling is not forbidden; where the SSH model's chiral symmetry related to sublattice isolation, the QSHE relates to preserving pseudo-spin [6, 16]. The off-diagonal, or imaginary parts, correspond to xy coupling [SH]. Suppose (r,s) is a lattice site. $x_{r,s}$ and $y_{r,s}$ are 1D oscillators in one unit cell at location (r,s); therefore, one cell is a two-dimensional oscillator [6]. U allows us to see how the array's eigenmodes are associated with clockwise and counter-clockwise polarized motion, defined as $\alpha = \pm$ [6]. These chiral modes are to this classical oscillator problem as pseudo-spin up and down are to the quantum problem

presented in the QSHE. What QSHE would consider spin up (down), this problem considers right (left) polarized edge mode [6]. It is $\mathcal{D}$ that will demonstrate QSHE properties through time reversal symmetry and the two chiral edge modes [6, 19].

To understand how time reversal and pseudo-spin symmetries observed in the QSHE for a spin-1/2 quantum state are understood in the case of classical mechanical oscillators, a latitude and longitude are mapped on the Bloch sphere. These are $\varphi = [\frac{-\pi}{2}, \frac{\pi}{2}]$ and $\theta = [0, 2\pi)$ respectively [6]. Such a state can be written as

$$|\psi\rangle = sin(\frac{\varphi + \frac{\pi}{2}}{2}) |\uparrow\rangle + e^{i\theta} cos(\frac{\varphi + \frac{\pi}{2}}{2}) |\downarrow\rangle \tag{58}$$

Time reversal moves a point on the Bloch sphere to its anti-nodal point, or a flip along both the latitude and longitude of the sphere $\mathcal{T} : (\varphi, \theta) \rightarrow (-\varphi, \theta + \pi)$, whereas pseudo-spin symmetry only causes a flip along the longitude $\sigma_z : (\varphi, \theta) \rightarrow (\varphi, \theta + \pi)$ [6]. In this way, the mapping of time reversal symmetry in QSHE to symmetries in an array of mechanical oscillators is

$$\mathcal{T} \rightarrow s \circ \mathcal{T} \tag{59}$$

where s represents the symmetry found in local modes of a unit cell, such that $s : (x, y) \rightarrow (y, -x)$ [6].

The assumption Süsstrunk and Huber make is that both s and $\mathcal{T}$ are independently true, or rather that there is no coupling between the left and right circular modes. They do briefly mention the possibility that this is not true. In such an instance $s \circ \mathcal{T}$ is still a symmetry of the system, but s and $\mathcal{T}$ are not symmetries on their own [6]. Süsstrunk and Hubers' consensus is that this latter symmetry scenario is not applicable to pendula [6]. Whether or not it is applicable to LC resonators is something to be determined. What is definitely applicable, though, is the general symmetry analysis comparing classical oscillators to the QSHE, as well as how the coupling matrix or Hamiltonian of the system is generated. The remaining questions regarding precisely how an array of LC resonators behaves in a similar set up will be outlined in the next section.

4 Research Questions and Project Scope

4.1 Research Questions

Goal

Find a model explaining how a two-dimensional array of LC resonators can act as a qubit.

Broader Questions

How could single qubit gates be run on this proposed system?

What does it mean for the system to be in superposition?

Narrower Questions

What is the lifetime of the edge modes and is that sufficient to enact a single qubit gate?

How is dissipation of the edge modes handled? Every system has its own sources of decay. Though this proposed hardware should be more robust to external noise, it very well may still have its own yet undiagnosed sources of decay. How can these effects be minimized through system control? What type of microwave pulses are required to maintain strong edge modes?

Similarly, what type of pulses are required to perform single qubit gates?

Which optimization methods best suit this problem of finding the best pulse for each scenario?

4.2 Project Plan

The following is an initial outline of the intended research plan. It is drafted to accommodate the dynamical nature of research and also with the knowledge that thoroughly defining a robust model for controlling the proposed hardware within a few months is a challenging task.

1) Verify already existing notebooks showing edge modes on 2D array is truly topologically invariant by removing sites along the physical edge of the array and still seeing edge modes present. This step has already begun.

2) Quantify lifetime of the edge modes and compare to necessary lifetime required to run a single qubit gate (particularly the X gate). If modes are sufficiently "strong", proceed to step 4. In all likelihood, will proceed to step 3.

3) Explore pulse optimization for exciting long lasting edge modes

4) Explore pulse optimization for manipulating edge modes to demonstrate a

single qubit gate. The first gate to explore will likely be the X, followed by the Z. If time allows, then the more complicated, yet interesting H gate will also be considered.

We will consider attaching two transmons to the array to excite and control the edge modes as shown in Figure 1 [5]. This would require integrating the Jaynes-Cummings Hamiltonian as presented in section 2.3. As previously mentioned, ultimately microwave pulses will be required to control the array. Pulse optimization will require exploration into various computational methods including, possibly, gradient ascent [21, 22, 23] and reinforcement learning [11].

There is also the option to make this system more realistic by incorporating representations of experimentally observed noise into the model. This does not seem to be an immediate priority, but as the project develops and the research needs adapt accordingly, this may be considered.

It should be noted that there is the possibility that steps 3 and 4 could be merged. Perhaps the pulse optimization in step 4 would also directly solve the problem step 3 is designed to address. This may become clearer after step 2 is completed.

The intention is to maintain clear notes throughout the whole process. This will aid in writing the final thesis, as well as assist other researchers in continuing this work more easily afterwards.

4.3 Predicting Challenges

While this report has laid out the theoretical argument for how this hardware should be able to apply topological edge modes to the classical circuit element that is the LC resonator, theory and experiment do not always precisely agree. Süsstrunk and Huber (2015) provided experimental agreement for demonstrating the QSHE on pendula and while pendula and LC resonators are similar, that does not guarantee with absolute certainty that LC resonators will demonstrate as clean results [6]. With that said, there has been evidence of the SSH model observed on a one-dimensional lattice of LC resonators. When transmons were paired with the resonators such that each resonator had one transmon attached to it, the qubits were able to be controlled by the edge states [24]. This evidence that topological symmetries were observed on a one-dimensional array of LC resonators and that this system was able to successfully manipulate qubits is another encouraging argument in support of this work.

With regards to particular aspects of the project plan, it is possible that step 3 will take the majority of the time. It may even be the bulk of this project if it is found crucial for understanding how to prepare and run gates (i.e. if the edge modes' lifetimes are not long enough to run gates as-is without assistance from extra pulses). If that is the case, the understanding that will have been gained in the process of solving step 3 will serve as very solid foundation for future work into pulse optimization for gates.

With that said, it is also possible that the optimal pulses for establishing long-lived edge modes and the optimal pulses for running gates do not necessarily agree once put together. Or rather, it is entirely possible that as these

two problems are being solved in a step-wise manner, there may exist an entire other pulse method that is not simply the combination of the two. This, however, will be reserved for future work. Quantum control can always be optimized in the eyes of today's researchers. The goal of this project is to build a good foundation for modeling the proposed hardware.

4.4 Timeline

April 2022
Literature review.
Step 1 of project plan.
Continue researching pulse optimization methods.

May - August 2022
Test pulse optimization methods.
Strengthen edge modes and determine X gate.
May 23-25, 2022: Present at COSSE workshop.
Continue with subsequent gates if time allows.
Write thesis.
August 2022: Thesis defense and final presentation.

Acknowledgements

Though it may not be traditional to put acknowledgements in literature reviews, no work is ever done in isolation. I would like to thank my committee for their support, encouragement, and patience thus far. Additionally, Guliuxin Jin has been incredible in answering my many questions regarding topological insulators and Overleaf. André Melo and Anthony Polloreno have graciously provided many helpful sanity checks throughout this learning process. Dylan Everingham and Mirko Kemna, as well as the whole QMAI group have created enlightening, enjoyable, and humane academic communities of which I am grateful to be a part. And finally, Marcus Palmer de Silva for recently reminding me that "perfect is an enemy of good enough."

References

[1] O. Dial. Eagle's quantum performance progress, Mar 2022.

[2] F. Arute, K. Arya, R. Babbush, et al. Quantum supremacy using a programmable superconducting processor. *Nature*, 574:505–510, 2019.

[3] C. Nayak. Microsoft has demonstrated the underlying physics required to create a new kind of qubit, Mar 2022.

[4] Microsoft Quantum Team. Developing a topological qubit, Sep 2018.

[5] E. Greplová. Engineered topological quantum networks, March 2021.

[6] R. Süsstrunk and S. D. Huber. Observation of phononic helical edge states in a mechanical topological insulator. *Science*, 349(6243):47–50, 2015.

[7] M. A. Nielson and I. L. Chuang. *Quantum Computation and Quantum Information*. Cambridge University Press, 10th anniversary edition, 2010.

[8] S. M. Girvin. Circuit QED: Superconducting Qubits Coupled to Microwave Photons, 2014.

[9] D. M. Pozar. *Microwave Engineering*, chapter 2.1, pages 48–51. John Wiley & Sons, Inc., 4th edition, 2012.

[10] D. Morin. *Introduction to Classical Mechanics, With Problems and Solutions*, chapter 15. Cambridge University Press, 2008.

[11] C. R Hoffer. Superconducting qubit readout pulse optimization using deep reinforcement learning. Master's thesis, Massachusetts Institute of Technology, Feb 2021.

[12] D. I. Schuster. *Circuit Quantum Electrodynamics*. PhD thesis, Yale University, May 2007.

[13] C. L. Kane and E. J. Mele. Quantum spin hall effect in graphene. *Phys. Rev. Lett.*, 95:226801, Nov 2005.

[14] A. Akhmerov, J. Sau, B. van Heck, et al. Topology in condensed matter: Tying quantum knots, 2021.

[15] W. P. Su, J. R. Schrieffer, and A. J. Heeger. Solitons in polyacetylene. *Phys. Rev. Lett.*, 42:1698–1701, Jun 1979.

[16] A. Pályi J. K. Asbóth, L. Oroszlány. *A Short Course on Topological Insulators*, volume 919 of *Lecture Notes in Physics*. Springer International Publishing, 2016.

[17] J. Larson and T. Mavrogordatos. *The Jaynes–Cummings Model and Its Descendants*. IOP Publishing, Dec 2021.

[18] R. Shankar. Topological insulators – a review, 2018.

[19] S. Huber. Mechanical metamaterials, 2018.

[20] B. Lian. Hofstadter butterfly: a momentum space method, and topological effects, Dec 2020.

[21] N. Khaneja, T. Reiss, C. Kehlet, et al. Optimal control of coupled spin dynamics: design of NMR pulse sequences by gradient ascent algorithms. *Journal of Magnetic Resonance*, 172(2):296–305, 2005.

[22] P. de Fouquieres, S.G. Schirmer, S.J. Glaser, et al. Second order gradient ascent pulse engineering. *Journal of Magnetic Resonance*, 212(2):412–417, 2011.

[23] R. W. Heeres, P. Reinhold, N. Ofek, et al. Implementing a universal gate set on a logical qubit encoded in an oscillator. *Nature Communications*, 8(1), Jul 2017.

[24] E. Kim, X. Zhang, V. S. Ferreira, et al. Quantum electrodynamics in a topological waveguide. *Physical Review X*, 11(1), Jan 2021.